Biomechanics and Modelling in Mechanobiology manuscript No.
(will be inserted by the editor)

Elastic properties of woven bone: effect of mineral content and collagen fibrils orientation

J. García-Rodriguez · J. Martínez-Reina

Received: date / Accepted: date

Abstract Woven bone is a type of tissue that forms mainly during fracture healing or foetal bone development. Its microstructure can be modelled as a composite with a matrix of mineral (hydroxyapatite) and inclusions of collagen fibrils with a more or less random orientation. In the present study its elastic properties were estimated as a function of composition (degree of mineralization) and fibril orientation. A self-consistent homogenization scheme considering randomness of inclusions' orientation was used for this purpose. Lacuno-canalicular porosity in the form of periodically distributed void inclusions was also considered. Assuming collagen fibrils to be uniformly oriented in all directions led to an isotropic tissue with a Young's modulus $E = 1.90\,GPa$, which is of the same order of magnitude as that of woven bone in fracture calluses. By contrast, assuming fibrils to have a preferential orientation resulted in a Young's modulus in the preferential direction of $9 - 16\,GPa$ depending on the mineral content of the tissue. These results are consistent with experimental evidence for woven bone in foetuses, where collagen fibrils are aligned to a certain extent.

Keywords Woven bone · Multiscale micromechanical model · Homegenization · Mineral content

1 Introduction

Woven bone is a type of tissue that appears when osteoblasts produce osteoid very rapidly. It is typically present in foetuses, in calluses during fracture healing, in individuals suffering from Paget's disease and in response to the

J. Martínez-Reina
Department of Mechanical Engineering, Universidad de Sevilla, Spain
Tel.: +34-954481365
E-mail: jmreina@us.es

administration of anabolic drugs in high doses (Su et al, 1997; Buckwalter et al, 1995; Zhou et al, 2001).

Mineralization causes composition changes in woven bone (Remaggi et al, 1998; Frost, 1989a,b; Su et al, 1997), which also experiences microstructural changes by effect of its replacement by lamellar bone during bone remodelling (Vetter et al, 2010, 2011; Sfeir et al, 2005; Brighton and Hunt, 1986, 1997). Like other types of bone tissue, woven bone consists of an inorganic phase (hydroxyapatite crystals), an organic phase (type I collagen, mainly) and water. Before remodelling, woven bone is microstructurally similar to many composite materials. Thus, it contains a matrix of wet mineral and more or less randomly oriented wet collagen fibrils (Smith, 1960) (see Fig. 1). The amount of mineral varies widely given that the newly deposited tissue (osteoid) consists only of collagen and water and, with time, this tissue mineralizes as water is replaced with mineral to a volume fraction of about 40%. Regarding the fibrils orientation, although they are most often assumed to be disordered, Su et al (1997) found a certain longitudinal alignment in long bones of foetuses.

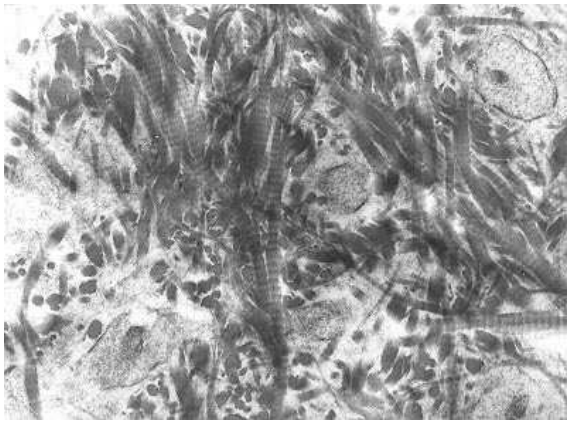

Fig. 1 Scanning electron micrograph of woven tissue showing disorderly arranged collagen fibrils. Reproduced from Hunt (Accessed 10 March 2016).

A sound knowledge of the mechanical properties of woven bone is paramount for some clinical uses such as the design of external fixators. Some fractures require using a fixator and the ratio between the stiffnesses of the fixator and the fracture callus has a decisive influence on the stress woven bone must withstand, which in turn influences how effectively it is remodelled and the fracture repaired. Designing effective fixators therefore requires knowing not only the mechanical properties of woven bone, but also the way they change during fracture healing.

In recent years, a number of authors have developed micromechanical models of lamelar bone, but none for woven bone as far as we know. Most of the models for lamellar bone use multiscale homogenization techniques (Deuerling et al, 2009; Dong and Guo, 2006; Ghanbari and Naghdabadi, 2009; Kotha

and Guzelsu, 2007; Porter, 2004; Sevostianov and Kachanov, 2000; Fritsch and Hellmich, 2007; Hellmich and Ulm, 2002; Hellmich et al, 2004). Lamellar bone has a hierarchical organization, from the nano scale (mineral crystals, collagen fibrils and water) to the micro scale (mineralized collagen fibers and lamella) that was carefully described by Yoon and Cowin in their micromechanical model (Yoon and Cowin, 2008b,a). That model was subsequently extended by Martínez-Reina et al (2011) to include the variation of mineral content during mineralization.

The primary aim of this work was to develop a multiscale homogenization model for estimating the mechanical properties of woven bone as a function of mineral content. For this purpose, we adapted a previously developed model for lamellar bone (Martínez-Reina et al, 2011) to the particular microstructure of woven bone. The proposed model was used to assess the influence of potential alignment of collagen fibrils in preferential directions as previously found by Su et al (1997) in foetal woven bone. Model-estimated results were compared with reported experimental values.

2 Materials and Methods

The proposed model is schematized in Fig. 2. There is little knowledge about the microstructure of woven bone other than that it is more disordered than lamellar bone by effect of much faster osteoid deposition. For this reason, we assumed its microstructure not to be as hierarchical as in lamellar tissue; thus, we considered none of the typical intermediate structures of lamellar tissue (lamellae, osteons). Rather, the compact woven tissue (before including the lacuno-canalicular porosity) was assumed to be a composite consisting of a matrix of wet mineral containing inclusions of wet collagen fibrils with a given probability distribution. Finally, the compact woven tissue was assumed to contain the lacuno-canalicular porosity hosting osteocytes, which are also present in woven bone and in a higher proportion than in lamellar tissue according to Remaggi et al (1998).

2.1 Basic components

Bone tissue consists basically of hydroxyapatite crystals (h), type I collagen (c) and water (w). Its composition can be described by:

$$v_i = \frac{V_i}{V_h + V_c + V_w} \qquad \text{with} \qquad v_h + v_c + v_w = 1 \tag{1}$$

where v_i and V_i are, respectively, the volume fraction and total volume of component $i = h, c, w$. The ash fraction, α, is defined as the ratio of the ash mass (mineral) to dry mass (mineral plus collagen):

$$\alpha = \frac{\rho_h v_h}{\rho_h v_h + \rho_c v_c} \tag{2}$$

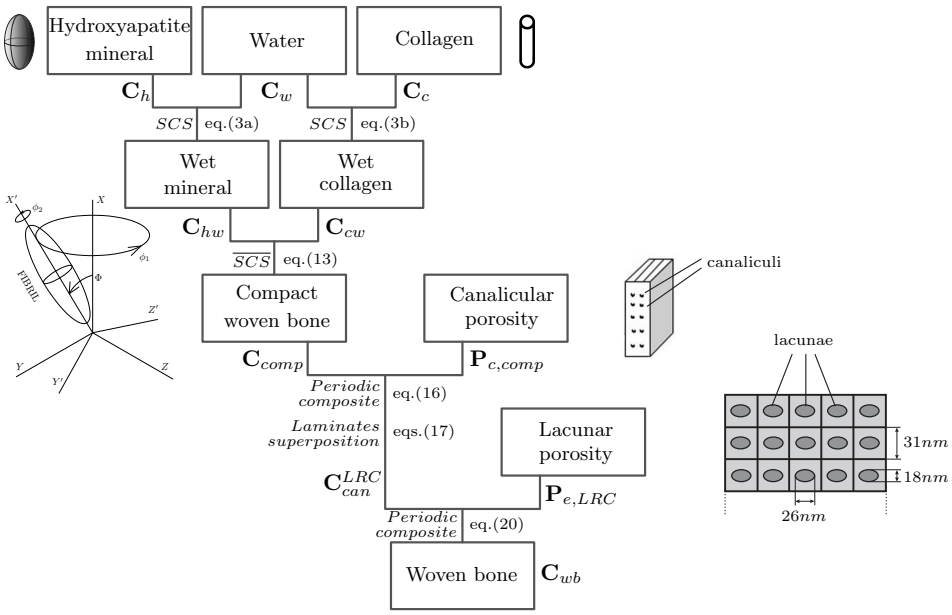

Fig. 2 Scheme of the proposed multiscale homogenization model.

where ρ_i designates the densities of the components. The basic components (mineral, collagen and water) were assumed to be isotropic (Katz, 1968; Crolet et al, 1993) and their stiffness tensors ($\mathbf{C}_h$, $\mathbf{C}_c$, $\mathbf{C}_w$) were defined in terms of the Young's moduli (E_i) and Poisson's coefficients (ν_i) given in Table 1. Water was modelled as in (Yoon and Cowin, 2008b; Martínez-Reina et al, 2011) and assumed to be an elastic material with a compressibility modulus $K_w = 2.3\,GPa$, which is typical of salt water, and a Poisson's coefficient close enough to 0.5 for E_w to be several orders of magnitude smaller than K_w, but not so small as to introduce numerical errors in the calculations.

	Elastic constants	
Mineral (hydroxyapatite)	$E_h = 114\,GPa$	$\nu_h = 0.28$
Water	$K_w = 2.3\,GPa$	$\nu_w = 0.4999$
Collagen	$E_c = 1.2\,GPa$	$\nu_c = 0.35$

Table 1 Elastic constants of the basic components. Taken from Katz (1968), Crolet et al (1993) and Yoon and Cowin (2008b).

2.2 Wet phases

Some water in the extracellular matrix was assumed to be trapped between the other basic components so to wet the mineral (Farlay et al, 2010) and the collagen fibrils (Grant et al, 2009). Thus, the wet phases were defined as in (Yoon and Cowin, 2008b) (viz., as collagen-water and mineral-water composites). In this work, however, we used a self-consistent scheme (SCS) to define the properties of the composites. This SCS is used when it is unclear which phase constitutes the matrix and which the inclusions or when the proportions of the two phases are similar (Hashin, 1968; Hill, 1965) and the hypothesis of dilute inclusions does not hold (e.g. in woven bone (García-Rodríguez, 2014)). The stiffness tensors for the wet mineral, $\mathbf{C}_{hw}$, and wet collagen $\mathbf{C}_{cw}$ were estimated from:

$$\mathbf{C}_{hw} = \mathbf{C}_w + \phi_{hw}\left(\mathbf{C}_h - \mathbf{C}_w\right)\left[\mathbf{I} + \mathbf{S}_{hw}\mathbf{C}_{hw}^{-1}\left(\mathbf{C}_h - \mathbf{C}_{hw}\right)\right]^{-1} \tag{3a}$$

$$\mathbf{C}_{cw} = \mathbf{C}_w + \phi_{cw}\left(\mathbf{C}_c - \mathbf{C}_w\right)\left[\mathbf{I} + \mathbf{S}_{cw}\mathbf{C}_{cw}^{-1}\left(\mathbf{C}_c - \mathbf{C}_{cw}\right)\right]^{-1} \tag{3b}$$

where ϕ_{hw} denotes the proportion of mineral present in the wet mineral composite and ϕ_{cw} that of collagen in the wet collagen composite. $\mathbf{S}_i$ denotes the Eshelby (Eshelby, 1957) tensor for each phase i. These equations are implicit and can be solved iteratively for $\mathbf{C}_{hw}$ and $\mathbf{C}_{cw}$. The first iteration involves assuming $\mathbf{C}_{hw}^0 = \mathbf{C}_w$ on the right-hand side of the equation and allows $\mathbf{C}_{hw}^1$ on the left-hand side to be calculated. In the second iteration, the resulting $\mathbf{C}_{hw}^1$ value is substituted on the right-hand side to obtain $\mathbf{C}_{hw}^2$ on the left-hand side. After a few iterations, the process converges to the tensor $\mathbf{C}_{hw}$. An identical result can be obtained by starting with the assumption $\mathbf{C}_{hw}^0 = \mathbf{C}_h$.

Eshelby's tensors (e.g., $\mathbf{S}_{hw}$) depend on the matrix stiffness tensor. Since the SCS formulation assumes the matrix to be the composite itself, the stiffness tensor for each iteration, $\mathbf{C}_{hw}^i$, is used as the matrix stiffness tensor needed to calculate $\mathbf{S}_{hw}$. Eshelby's formulation assumes inclusions to be ellipsoid-shaped and thus the tensors $\mathbf{S}_i$ depend on the ellipsoid dimensions. The inclusions of the wet collagen composite are collagen fibrils that are assumed to be infinitely long cylinders ($b = c$ and $a \to \infty$, where a, b and c are the semi-axes lengths of a generic ellipsoid). The inclusions of the wet mineral composite are hydroxyapatite crystals, which are parallelepiped in its pure form (Jackson et al, 1978) and preclude use of Eshelby's approach as a result. However, the lack of stoichiometry, confirmed by García-Rodríguez (2014) in woven bone, makes the crystals to be amorphous (Farlay et al, 2010). For this reason, mineral inclusions were approximated by ellipsoids whose semi-axes lengths were taken from measurements of crystals made by Su et al (2003) in human foetal woven bone: $a = 32\,nm$, $b = 19\,nm$, $c = 3\,nm$.

The proportion of mineral in the wet mineral phase, ϕ_{hw}, was taken as:

$$\phi_{hw} = \frac{v_h}{v_h + v_{wh}} \tag{4}$$

where v_{wh} is the water volume fraction in the wet mineral phase. If, as previously assumed by Martínez-Reina et al (2011), water binds to mineral and collagen in proportion to the volume of each, then:

$$v_{wh} = v_w \frac{v_h}{v_h + v_c} \tag{5}$$

substitution of which into (4) yields:

$$\phi_{hw} = 1 - v_w \tag{6}$$

A similar procedure can be used to calculate the proportion of collagen in the wet collagen phase, which coincides with ϕ_{hw}:

$$\phi_{cw} = \phi_{hw} = 1 - v_w \tag{7}$$

The composition of woven tissue changes with time. Freshly deposited osteoid contains water and collagen only, so $v_h = 0$. As tissue mineralizes, water is replaced by mineral, deposited between collagen fibrils. As a result, the volume of organic phase remains constant and identical with its volume within the osteoid (i.e., $v_c = constant$). The collagen volume fraction used in this work, $v_c = 0.593$, was measured in sheep distraction calluses (García-Rodríguez, 2014) and assumed to remain constant until remodelling starts. At that point, the old woven tissue will be progressively resorbed and replaced by fresh lamellar tissue, with a different composition and microstructure. Consequently, the proposed model is time-limited and will only hold until woven tissue starts to be remodelled. After that point the model should consider a mixture of woven and lamellar tissue, which is beyond the scope of this work.

Mineralization in lamellar tissue is initially fast during the so-called "primary" mineralization phase and then slows down as the tissue becomes saturated with mineral in the "secondary" mineralization phase. The process can last 6 months to several years (Parfitt, 1987) until complete saturation, which occurs at about $\alpha = 0.7$ (Hernandez et al, 2001b; García-Aznar et al, 2005). Regarding woven tissue, its saturated ash fraction and mineralization rate are unknown, though it is probably remodelled prior to saturation. In fact, Vetter et al (2010) found signs of remodelling just 8 weeks after formation. Therefore, the aforementioned time limitation of the model makes it inapplicable well before the tissue is saturated with mineral. For generality, however, we assumed v_h to range from 0 to $v_{h,sat}$. The latter value was estimated from the constant $v_c = 0.593$ under the assumption that the amount of water remaining in the tissue was virtually negligible: $v_{w,min} = 0.01$.

$$v_{h,sat} = 1 - v_c - v_{w,min} = 0.406 \quad \Leftrightarrow \quad \alpha_{sat} = 0.603 \tag{8}$$

where (2) was used.

2.3 Stiffness tensor of compact woven tissue

Woven tissue was modelled as a composite formed by wet mineral and wet collagen phases, the stiffness tensors of which, $\mathbf{C}_{hw}$ and $\mathbf{C}_{cw}$, were used to estimate the properties of compact woven tissue (before including the lacuno-canalicular porosity). With normal ash fraction values, the volume fractions of the two phases are typically very similar (García-Rodríguez, 2014). This precludes discriminating between the matrix and its inclusions in most cases and accepting the hypothesis of dilute inclusions underlying the Mori-Tanaka homogenization method in virtually all cases. We therefore had to use a self-consistent scheme (SCS) instead.

In woven tissue, collagen fibrils are more or less randomly oriented and mineral fills the gaps between fibrils. Some authors have used the Mori-Tanaka method to describe the elastic behaviour of composite materials consisting of a matrix and non-aligned inclusions (Benveniste, 1990; Pettermann et al, 1997; Ferrari and Johnson, 1989) in terms of orientation distribution functions (ODFs) or length distribution functions (LDFs). Ferrari and Johnson (1989) proposed using an averaged stiffness tensor depending on the probability density of the orientation of inclusions. Thus, for a generic tensor $\mathbf{F}(\mathbf{g})$ in a given direction represented by $(\mathbf{g})$, they defined the average tensor $\overline{\mathbf{F}}$ as:

$$\begin{aligned}\overline{\mathbf{F}} &= \oint \mathbf{F}(\mathbf{g})\rho(\mathbf{g})\mathrm{d}\mathbf{g} = \\ &= \frac{1}{\bar{\rho}}\int_0^{2\pi}\int_0^{\pi}\int_0^{2\pi}\mathbf{F}(\mathbf{g})\rho(\mathbf{g})\sin\Phi\ \mathrm{d}\phi_1\ \mathrm{d}\Phi\ \mathrm{d}\phi_2\end{aligned} \tag{9}$$

which uses Euler angles $\mathbf{g} = \{\Phi \in (0,\pi),\ \phi_1 \in (0,2\pi),\ \phi_2 \in (0,2\pi)\}$ to orientate inclusions (viz., collagen fibrils) as shown in Fig. 3. $\mathbf{F}(\mathbf{g})$ represents the generic tensor $\mathbf{F}$ upon rotation in the direction defined by $\mathbf{g}$, $\rho(\mathbf{g})$ a probability function for fibril orientation and $\bar{\rho}$ a constant defined later on. If the representative volume element (RVE) is assumed to have point symmetry, then $\rho(\mathbf{g})$ will be independent of ϕ_1 and ϕ_2. In addition, $\rho(\mathbf{g})$ should fulfil the following condition (Ferrari and Johnson, 1989; Bunge, 1982):

$$\oint \rho(\mathbf{g})\mathrm{d}\mathbf{g} = 1 \tag{10}$$

In this work, we assumed collagen fibrils to be oriented with a uniform probability density function in the RVE, i.e.,

$$\rho(\mathbf{g}) = \begin{cases}\rho = \text{constant} & \forall\Phi \in [\gamma_1,\gamma_2] \\ 0 & \text{elsewhere}\end{cases} \tag{11}$$

so that:

$$\oint \rho(\mathbf{g})\mathrm{d}\mathbf{g} = \frac{1}{\bar{\rho}} \int_0^{2\pi} \int_0^{\pi} \int_0^{2\pi} \rho(\Phi) \sin\Phi \, \mathrm{d}\phi_1 \, \mathrm{d}\Phi \, \mathrm{d}\phi_2 = \\ = \frac{4\rho\pi^2}{\bar{\rho}} \int_{\gamma_1}^{\gamma_2} \sin\Phi \, \mathrm{d}\Phi = 1 \tag{12}$$

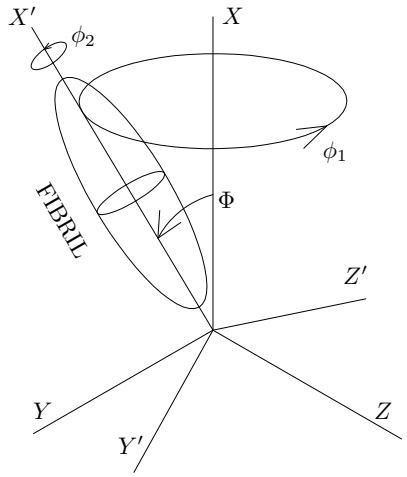

Fig. 3 Schematic depiction of fibril orientation showing the local axes ($X'Y'Z'$), global axes (XYZ) and the angles between them. The ellipsoid represents a fibril with an orientation $\mathbf{g} = \{\Phi, \phi_1, \phi_2\}$.

which can be easily solved for $\bar{\rho}$. The constituents water, mineral and collagen were assumed isotropic, then the wet phases will also be isotropic. As a result, rotating a fibril about ϕ_2 will have no effect on the previous equations, so (9) can be rewritten as:

$$\overline{\mathbf{F}} = \frac{1}{2\pi(\cos\gamma_1 - \cos\gamma_2)} \int_0^{2\pi} \int_{\gamma_1}^{\gamma_2} \mathbf{F}(\mathbf{g}) \sin\Phi \, \mathrm{d}\phi_1 \, \mathrm{d}\Phi \tag{13}$$

Ferrari and Johnson (1989) used the previous averaging procedure in the Mori-Tanaka method to estimate concentration tensors and hence stiffness tensors. In this work, we applied this procedure to a self-consistent scheme (SCS), analogously to what has been done in other works (Fritsch et al, 2006, 2013). Selection of the particular phases to be used as matrix and inclusions in the first iteration was crucial with non-aligned inclusions, for its strong impact on the results. In woven tissue, wet collagen fibrils are randomly oriented and appear to be surrounded by mineral filling the gaps left by the fibrils; therefore, it seems more reasonable to use wet collagen fibrils as inclusions

and wet mineral as the matrix. In this way, similarly to Ferrari and Johnson (1989), the stiffness tensor for compact woven tissue, $\mathbf{C}_{comp}$, can be defined as:

$$\mathbf{C}_{comp} = \mathbf{C}_{hw} + \xi \overline{(\mathbf{C}_{cw} - \mathbf{C}_{hw})\,\mathbf{A}_{comp}} \tag{14}$$

where the bar over $(\mathbf{C}_{cw} - \mathbf{C}_{hw})\,\mathbf{A}_{comp}$ means that this tensor is averaged using eq. (13). The concentration tensor is given by:

$$\mathbf{A}_{comp} = \left[\mathbf{I} + \mathbf{S}_{comp}\mathbf{C}_{comp}^{-1}\left(\mathbf{C}_{cw} - \mathbf{C}_{comp}\right)\right]^{-1} \tag{15}$$

where ξ is the volume fraction of inclusions (wet collagen) in the tissue and $\mathbf{S}_{comp}$ is the Eshelby tensor corresponding to ellipsoidal inclusions within a matrix of compact woven tissue. Again, calculating $\mathbf{C}_{comp}$ requires using an iterative procedure because the matrix in (15) is assumed to be the composite itself. This makes $\mathbf{C}_{comp}$ to appear in both sides of equation (14) (also in $\mathbf{S}_{comp}$ which depends on the matrix). The wet collagen inclusions are assumed to be cylinders of infinite length ($b = c$ and $a \to \infty$). Their volume fraction is given by:

$$\xi = v_c + v_{wc} = \frac{v_c + v_{wc}}{v_h + v_{wh} + v_c + v_{wc}} = \frac{v_c}{v_h + v_c} \tag{16}$$

where (5) and (7) have been used.

This model was also used to assess the influence of orientation in the collagen fibrils and their potential alignment in a specific direction, as previously observed by Su et al (1997) in foetal long bones, on the properties of woven tissue. In foetal long bones collagen fibrils are approximately aligned with the longitudinal direction. To take this into account revolution symmetry about an axis (X in Fig. 3) was assumed along with $\gamma_1 = 0$ (see Fig. 4a which converts into Fig. 4b for this special case). In addition, the orientation probability function was assumed uniform $\rho(\mathbf{g}) = \rho = constant$ in subdomain $\Phi \in [0, \gamma_2]$ (see Fig. 4b). If the collagen fibrils had no preferential orientations, but rather were uniformly distributed throughout the entire space, then $\gamma_2 = \pi/2$; on the other hand, if the fibrils were totally aligned in a preferential direction, then $\gamma_1 = \gamma_2 = 0$.

2.4 Properties of woven tissue including pores

In this step, the lacuno-canalicular porosity was included in the material. These pores are occupied by osteocytes which have a central body in the lacuna and processes in the canaliculi. Since lacunae and canaliculi differ in shape, they were dealt with separately as in previous studies (Martínez-Reina et al, 2011; Yoon and Cowin, 2008a).

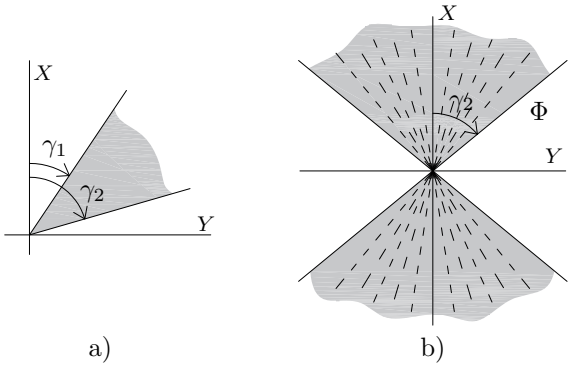

Fig. 4 Collagen fibrils with revolution symmetry about the X axis and a uniform probability function in the region $\Phi \in [\gamma_1, \gamma_2]$ in the most general case (a) and in the particular case dealt with here $\gamma_1 = 0$ (b).

2.4.1 Canalicular porosity

In this step, we estimated the properties of a composite with a matrix consisting of compact woven tissue of stiffness $\mathbf{C}_{comp}$ and void inclusions representing the canaliculi. These canaliculi were modelled as cylinders of infinite length periodically distributed in the longitudinal, radial and circumferential directions (Yoon and Cowin, 2008a). The method of Nemat-Nasser and Hori (Nemat-Nasser and Hori, 1999) for composites with periodic inclusions, of null stiffness in this case, provides:

$$\mathbf{C}^k_{can} = \mathbf{C}_{comp}\left[\mathbf{I} - p^{wov}_{can}\left(\mathbf{I} - \mathbf{P}^k_{c,comp}\right)^{-1}\right] \tag{17}$$

where p^{wov}_{can} denotes canalicular porosity, which is calculated below; $\mathbf{P}^k_{c,comp}$ is a 6x6 periodic tensor operator for infinitely long cylindrical inclusions (see Nemat-Nasser and Hori, 1999) embedded in a matrix of compact woven tissue described in Section 2.3; and $\mathbf{C}^k_{can}$ is the stiffness tensor including canalicular porosity in the k direction, which can be longitudinal (L), radial (R) or circumferential (C).

Following Yoon and Cowin (2008a), we superimposed three tissue laminates with canalicular porosity in the three directions (L, R and C), using the formulation of Chou et al (1972) for laminar composites. Thus, once the volume fraction for each laminate, V^k, is known, the stiffness tensor of the tissue with canalicular porosity, $\mathbf{C}^{LRC}_{can}$, can be determined. The components of this tensor are:

$$\begin{aligned} C^{LRC}_{can,ij} = \sum_{k=1}^{3} V^k \Bigg\{ & C^k_{can,ij} - \frac{C^k_{can,i3} C^k_{can,i3}}{C^k_{can,33}} + \\ & + \frac{C^k_{can,i3} \sum_{\Omega=1}^{3} \frac{V^\Omega C^\Omega_{can,3j}}{C^\Omega_{can,33}}}{C^k_{can,33} \sum_{\Omega=1}^{3} \frac{V^\Omega}{C^\Omega_{can,33}}} \Bigg\} \quad \forall\, i,j = 1,2,3,6 \end{aligned} \tag{18a}$$

$$C^{LRC}_{can,ij} = \frac{\sum_{k=1}^{3} \frac{V^k}{\Delta^k} C^k_{can,ij}}{\sum_{k=1}^{3} \sum_{\Omega=1}^{3} \frac{V^k V^\Omega}{\Delta^k \Delta^\Omega} \Gamma^{k\Omega}} \quad \forall\, i,j = 4,5 \tag{18b}$$

where

$$\Delta^k = C^k_{can,44} C^k_{can,55} - C^k_{can,45} C^k_{can,54} \tag{19a}$$

$$\Gamma^{k\Omega} = C^k_{can,44} C^\Omega_{can,55} - C^k_{can,45} C^\Omega_{can,54} \tag{19b}$$

corresponding the subscripts $k, \Omega = 1,2,3$ to the L, R and C directions, respectively. Since p^{wov}_{can} in (17) was taken the same $\forall k$, the proportion of canaliculi in each direction must be considered in equations (18a) and (18b) through V^k (Yoon and Cowin, 2008b; Beno et al, 2006).

The procedure used to estimate V^k is described in (Yoon and Cowin, 2008b). Canaliculi are assumed to run from the osteocyte normal to the lacuna and in no preferential direction. As a result, the number of canaliculi oriented in a given direction depends on the shape, dimensions and orientation of the lacuna. A lacuna is approximated to an ellipsoid aligned with the LRC directions and having the semi-axes lengths $2b_L = 13\,\mu m$, $2b_C = 12\,\mu m$ and $2b_R = 9\,\mu m$ in woven tissue (Remaggi et al, 1998). This allows the proportions V^k to be approximated to the ratios between the ellipsoid sections with the planes normal to each LRC direction. Thus,

$$V^L = \frac{b_C\, b_R}{b_C\, b_R + b_C\, b_L + b_L\, b_R} = 0.283 \tag{20}$$

A similar procedure yielded $V^C = 0.307$ and $V^R = 0.409$.

2.4.2 Lacunar porosity

Canalicular porosity was estimated by using an equation similar to (17) but applied to void ellipsoidal inclusions (lacunae):

$$\mathbf{C}_{wb} = \mathbf{C}^{LRC}_{can} \left[\mathbf{I} - p^{wov}_{lac} \left(\mathbf{I} - \mathbf{P}_{e,LRC} \right)^{-1} \right] \tag{21}$$

where $\mathbf{C}_{wb}$ is the final stiffness tensor for woven tissue -total porosity included-, p^{wov}_{lac} is the lacunar porosity, and $\mathbf{P}_{e,LRC}$ is the tensor operator for periodic ellipsoidal voids (see (Nemat-Nasser and Hori, 1999)) embedded in a matrix consisting of tissue with canalicular porosity.

In a periodic composite each inclusion is assumed to be contained in a periodically repeated cell unit of matrix (Nemat-Nasser and Hori, 1999). In lacunae, the unit cell is assumed to be a cube of edge length $2L^{wov}_{cell}$ (Yoon and Cowin, 2008b). Parameter p^{wov}_{lac} is obtained from the dimensions of the lacuna and unit cell. The former was approximated in Section 2.4.1 to an ellipsoid of volume

$$V^{wov}_{lac} = \frac{4}{3}\pi \cdot b_L \cdot b_R \cdot b_C = 735.1\,\mu m^3 \tag{22}$$

The dimensions of the unit cell were estimated by following Remaggi et al (1998), who used histomorphometric measurements to determine the average osteocyte density in woven bone from various species and found $A^{wov} =$

1050 osteocytes/mm^2 for humans. Based on this value, $2L_{cell}^{wov} = 1/\sqrt{A^{wov}} = 30.86\,\mu m$ (Beno et al, 2006), and hence the unit cell volume is $V_{cell}^{wov} = (2L_{cell}^{wov})^3 = 29391\,\mu m^3$. Together with (22), this allowed lacunar porosity to be estimated as $p_{lac}^{wov} = V_{lac}^{wov}/V_{cell}^{wov} = 0.0250$, which is much greater than the identically estimated value for lacunar porosity in human lamellar tissue: $p_{lac}^{lam} = 0.0082$.

The absence of reported values for p_{can}^{wov} led us to estimate it under some assumptions. Thus, lacuno-canalicular porosity was split into two terms:

$$p_{lc}^{wov} = p_{lac}^{wov} + p_{can}^{wov} \tag{23}$$

The total pore volume of the unit cell, V_{lc}^{wov}, is

$$V_{lc}^{wov} = V_{lac}^{wov} + V_{can}^{wov} = p_{lc}^{wov}\, V_{cell}^{wov} \tag{24}$$

where V_{lac}^{wov} and V_{can}^{wov} are, respectively, the lacunar and canalicular volume within the unit cell. Osteoblasts in woven and lamellar bone are assumed to be identical in size. When osteoblasts are buried in the bone matrix and differentiated to osteocytes, they change shape and leave a cell body and several cell processes that interconnect osteocytes to one another. As a result, the osteocyte volume distributes between the lacunar volume (cell body) and the canalicular volume (cell processes). Although the difference between p_{lac}^{wov} and p_{lac}^{lam} suggests that porosity of lamellar and woven tissue may be unequally distributed, in this work we assumed the total pore volume, V_{lc}, to be the same in both if their osteoblasts are of the same size, as assumed above, i.e.,

$$V_{lc}^{lam} = V_{lc}^{wov} \quad \Leftrightarrow \quad p_{lc}^{lam} \cdot V_{cell}^{lam} = p_{lc}^{wov} \cdot V_{cell}^{wov} \tag{25}$$

A combination of (23) and (25) yields

$$p_{can}^{wov} = p_{lc}^{wov} - p_{lac}^{wov} = p_{lc}^{lam} \frac{V_{cell}^{lam}}{V_{cell}^{wov}} - p_{lac}^{wov} = 0.1103 \tag{26}$$

The previously estimated V_{cell}^{wov} and p_{lac}^{wov} were substituted in the last equation, together with the value $p_{lc}^{lam} = 0.05$, which was taken after (Yoon and Cowin, 2008a; Cowin, 1999; Wang et al, 1999; Zhang and Cowin, 1994; Zhang et al, 1998). Finally, the dimension of the unit cell in lamellar tissue $2L_{celda}^{lam} = 43\,\mu m$, estimated by Beno et al (2006) from the results of Remaggi et al (1998) for lamellar tissue in cortical bone, yields $V_{cell}^{lam} = (2L_{celda}^{lam})^3 = 76507\,\mu m^3$, which allowed to estimate p_{can}^{wov} in (26).

It should be noted that the lacuno-canalicular porosity in woven tissue, $p_{lc}^{wov} = 0.1353$, is considerably greater than in lamellar tissue of cortical bone ($p_{lc}^{lam} = 0.05$). The difference can be ascribed to the nature of woven tissue, which contains much more collagen than lamellar tissue (García-Rodríguez, 2014) as the likely result of having a higher concentration of osteoblasts. One can therefore expect the amount of osteoblasts buried in the bone matrix and differented to osteocytes to be greater in woven tissue than in lamellar tissue, which is consistent with the experimental osteocyte density measurements of Hernandez et al (2004) and Remaggi et al (1998).

2.5 Volumetric composition of woven tissue

Applying the equations of the proposed model entails knowing the volumetric composition of woven tissue. In a previous study, 11 sheep (merino breed, 3 to 5 years old) were subjected to metatarsal bone transport (Mora-Macías et al, 2016). During the healing period the woven tissue mineralizes and is remodelled (and replaced with lamellar tissue) in the long term. The sheep were sacrificed at different stages of the healing process and two woven tissue specimens obtained from the gap zone of each animal. One of the two specimens was analyzed histomorphometrically in order to discard those sheep with signs of bone remodelling (López-Pliego et al, 2015). The other specimen from those sheep exhibiting no such signs was used to determine the volumetric composition of woven tissue according to García-Rodríguez (2014). A lamellar tissue specimen from the cortical layer of the contralateral metatarsus was also obtained for comparison. The latter was extracted at the same position of the gap of the operated metatarsus in such sheep. Table 2 compares the average volumetric composition results with previously reported values of Gong et al (1964) for lamellar tissue from human cortical bone. The mineral content of tissue is usually measured with the ash fraction, which is also shown in the table, and calculated as

$$\alpha = \frac{m_m}{m_m + m_o} = \frac{\rho_m \, v_m}{\rho_m \, v_m + \rho_o \, v_o} \tag{27}$$

where m, v and ρ represent mass, volume and density, respectively, and the subscripts m and o denote mineral and organic phase, respectively. The values $\rho_m = 3.12\, g/cm^3$ and $\rho_o = 1.43\, g/cm^3$ were used (Lees et al, 1979).

	Mineral v_h	Organic phase v_c	Water v_w	Ash fraction α
Woven bone (Sheep) [a]	0.280	0.584	0.136	0.511
Lamellar bone (Sheep) [a]	0.398	0.392	0.210	0.689
Lamellar bone (Human) [b]	0.395	0.354	0.251	0.709

Table 2 Volumetric composition and ash fraction of various types of woven tissue. Results from (a) García-Rodríguez (2014), (b) Gong et al (1964).

3 Results

Table 3 shows the stiffness results for sheep woven tissue as estimated from volumetric composition data under the assumption that collagen fibrils were oriented with an identical probability in all directions ($\gamma_2 = \pi/2$). Formally, the proposed method provides an orthotropic stiffness tensor $\mathbf{C}_{wb}$ which, however, is quasi-isotropic with $\gamma_2 = \pi/2$. This fact was exploited by using the

symmetrization method of Cowin and coworkers (Yang et al, 1998; Cowin et al, 1999; Yoon et al, 2002), who proposed an isotropic estimate of the stiffness tensor obtained by averaging the classical estimates of Voigt and Reuss. This approximation yields the Young's modulus and Poisson's coefficient shown in Table 3 for $\gamma_2 = \pi/2$.

Orthotropic constants		**Isotropic constants**	
E_1	1.8318 GPa		
E_2	1.9647 GPa	E	1.9041 GPa
E_3	1.8605 GPa		
ν_{12}	0.3552		
ν_{13}	0.3410		
ν_{21}	0.3520	ν	0.3431
ν_{23}	0.3565		
ν_{31}	0.3355		
ν_{32}	0.3375		
G_4	0.7114 GPa		
G_5	0.7086 GPa	G	0.7088 GPa
G_6	0.7207 GPa		

Table 3 Estimated elastic constants for woven tissue before (orthotropic) and after (isotropic) symmetrization with the method of Cowin et al (1999). The volumetric composition is that given in Table 2 for woven bone and $\gamma_2 = \pi/2$.

We also examined the variation of $\mathbf{C}_{wb}$ with composition during the mineralization process. Fig. 5 shows the variation of the elastic constants with the ash fraction in the equivalent isotropic material obtained by symmetrizing $\mathbf{C}_{wb}$. The figure also shows various fitted elastic constant-ash fraction curves.

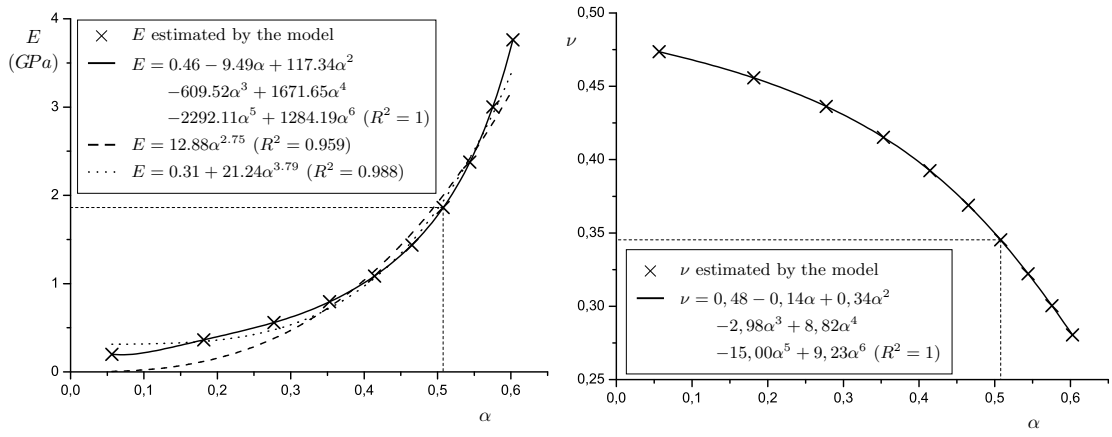

Fig. 5 Variation of Young's modulus and Poisson's coefficient of the equivalent isotropic material with the ash fraction, α, for $\gamma_2 = \pi/2$.

The influence of alignment of collagen fibrils was assessed by examining the variation of the stiffness tensor $\mathbf{C}_{wb}$ with angle γ_2 for the sheep volumetric composition ($\alpha = 0.511$, see Table 2) and for other three greater values of α.

The tensor was orthotropic and the Young's moduli in the three orthotropic directions are shown in Fig. 6, where X, Y and Z in Fig. 3 correspond to E_1, E_2 and E_3, respectively. As can be seen, clustering of collagen fibrils in a given direction (i.e., a decrease in γ_2) led to increased stiffness in that direction but had virtually no effect on the stiffness in the other orthotropic directions. The symmetry of the estimated stiffness tensor for woven tissue is very close to transverse isotropy, which is consistent with the expectations because, as can be seen from Fig. 3 and Eq. (13)), the model does not depend on ϕ_1. The above-mentioned symmetrization technique (Yang et al, 1998; Cowin et al, 1999; Yoon et al, 2002) allowed us to obtain an equivalent transversely isotropic material with a stiffness tensor $\mathbf{C}_{wb}^{TI}$. Table 4 shows the Young's moduli in the longitudinal direction X, termed E_l, and in the transversal direction of the symmetry plane, E_t, at different α and γ_2 values. The fact that $\mathbf{C}_{wb}$ was quasi-transversely isotropic was confirmed by calculating the following parameter that measures the difference between the original and the symmetrized tensors:

$$dif(\%) = \frac{||\mathbf{C}_{wb}^{TI} - \mathbf{C}_{wb}||}{||\mathbf{C}_{wb}||} \cdot 100 \tag{28}$$

where the norm of the tensor is defined as

$$||\mathbf{C}|| = \sqrt{\mathbf{C} : \mathbf{C}} = \sqrt{\sum_{i=1}^{6}\sum_{j=1}^{6} C_{ij}^2} \tag{29}$$

It was checked that dif never exceeded 2% being these differences due only to the numerical integration of equations such as (13).

γ_2	$\alpha = 0.511$		$\alpha = 0.530$		$\alpha = 0.555$		$\alpha = 0.580$	
	E_l	E_t	E_l	E_t	E_l	E_t	E_l	E_t
$\pi/18$	9.31	1.70	10.76	1.89	13.14	2.19	16.15	2.56
$\pi/6$	3.25	1.73	3.75	1.93	4.61	2.26	5.74	2.67
$\pi/3$	2.06	1.84	2.34	2.07	2.79	2.46	3.39	2.96
$\pi/2$	1.86	1.93	2.10	2.18	2.49	2.60	2.99	3.16

Table 4 Longitudinal (E_l) and transverse (E_t) Young's modulus, in GPa, of the equivalent transversely isotropic material.

Fig. 7 shows the variation of E_l and E_t with α in the equivalent isotropic material with quasi-aligned fibrils. Specifically, γ_2 was assumed to be $\pi/18$, which is small enough to simulate quasi-aligned fibrils but allowed the integrals in Eq. (13) to be solved in the case $\gamma_1 = 0$ without numerical problems.

4 Discussion

The elastic properties of composites containing randomly arranged inclusions -which is the case with woven bone in most cases-, are usually worked out

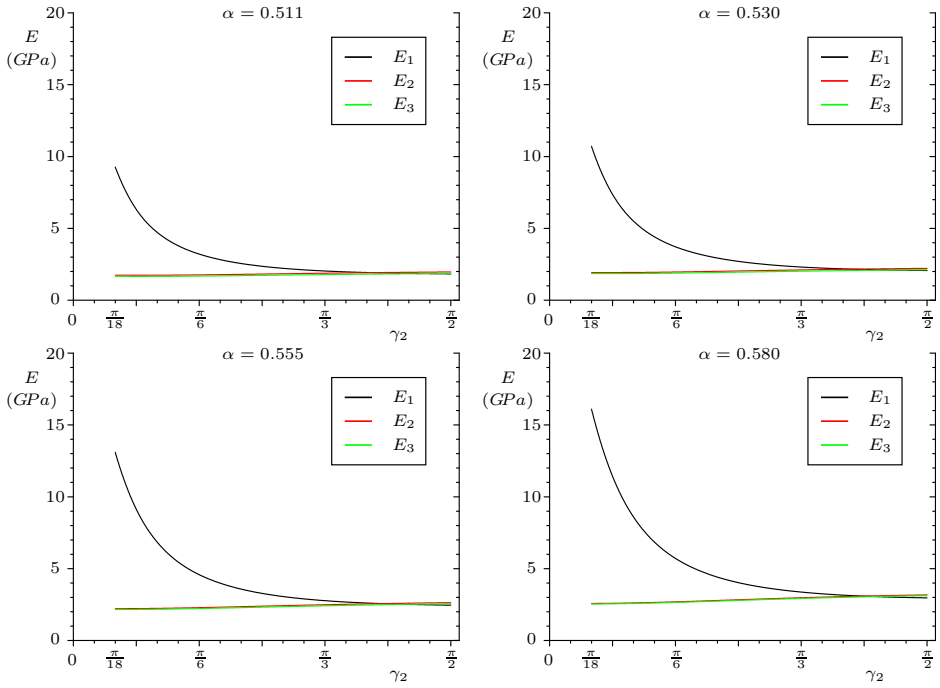

Fig. 6 Variation of the estimated Young's moduli in the three orthotropic directions with angle γ_2 and the ash fraction α.

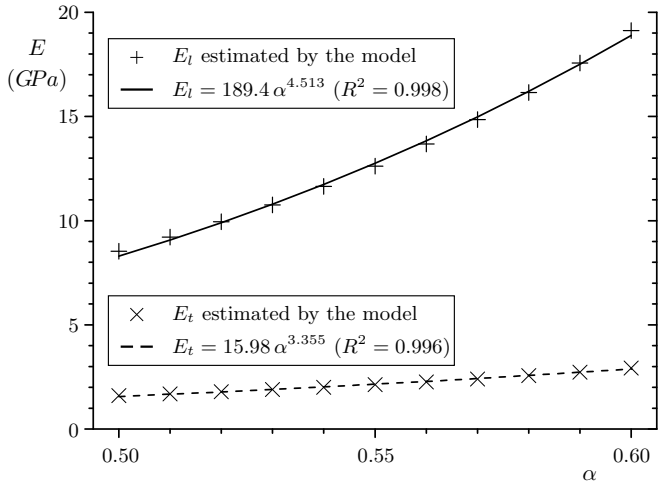

Fig. 7 Variation of the Young's moduli of the equivalent transversely isotropic material with the ash fraction at an angle $\gamma_2 = \pi/18$ and fitted exponential curve for each modulus.

with a rule of mixtures in order to considerably reduce the numerical effort. Using the average composition of woven tissue as measured in sheep (see Table 2) provided a Voigt estimation (weighted volume average of the stiffness of constituent phases) $E_{Voigt} = 32.7\,GPa$, which is an upper bound of the Young's modulus for the composite. On the other hand, the Reuss estimation (weighted volume average of the compliance of constituent phases) provided $E_{Reuss} = 0.01\,GPa$, which is a lower bound. Some authors have proposed using the average of the two bounds as an estimation of composite's elastic modulus (Yoon and Cowin, 2008b); however, this makes no sense here owing to their large difference -a result of the also large difference in stiffness between constituents. Rather, woven tissue requires using a more complex choice such as the proposed model, which considers the microstructure of the composite and the more or less random orientation of the inclusions.

The proposed micromechanical model predicts an orthotropic behaviour for woven tissue. However, as can be seen from Table 3, the results suggest a quasi-isotropic behaviour for $\gamma_2 = \pi/2$. The reason for this symmetry is the way wet collagen fibrils are assumed in that case, with a uniformly random distribution throughout the entire space.

The elastic properties of woven tissue are clearly dependent on its mineral content, as can be seen from Fig. 5. Mineralization markedly increases stiffness and decreases Poisson's coefficient as a result of mineral replacing water initially present in the tissue. Moreover, mineralization in woven tissue is especially fast (García-Rodríguez, 2014), likely by effect of its high content in type I collagen, which favours deposition of mineral. Therefore, based on the proposed model, bone callus may recover its stiffness very rapidly during fracture healing, which is a functionally optimal result.

As can also be seen from Fig. 5, the polynomial equation was the best option to fit the Young's modulus versus the ash fraction (the degree 6 was the lowest providing $R^2 \simeq 1$). The other two curves in the figure were used for comparison with the experimental results of Hernandez et al (2001a), who obtained:

$$E\,(GPa) = 84.37 v_b^{2.58} \alpha^{2.74} \tag{30}$$

The exponential regression curves with a constant term ($E = A\,\alpha^B + C$, where constants A, B and C were fitted) resulted in slightly better fitting than a simple exponential regression equation ($E = A\,\alpha^B$); interestingly, however, the exponent of the latter coincided with that of the correlation of Hernandez et al (2001a), which also lacks a constant term, despite the fact that these authors tested lamellar tissue. Therefore, the elastic properties of both types of tissue must be similarly influenced by the mineral phase.

Very few authors have reported experimental measurements of stiffness in woven tissue. Among the few are Leong and Morgan (2008), who performed nanoindentation tests on fracture calluses in rat femurs. Their results were widely variable with location within the callus ($26.92 - 1010\,MPa$). Gardner et al (2000) estimated the Young's modulus of woven tissue during healing of a

tibial fracture in a 20-year-old individual by using inverse finite element characterization. They split the fracture region into very wide zones and obtained Young's modulus ranging from 500 to 3600 MPa depending on the particular zone and the time after fracture. These values exceed those of Leong and Morgan, possibly because the measurements of Gardner et al. included late healing stages where the fracture might already have undergone remodelling in some regions and, thus, mineralized lamellar tissue had appeared. However, both ranges of values are consistent with our estimates, especially with those for the average composition of sheep woven tissue and for quasi-isotropic tissue (i.e., tissue with randomly oriented fibrils).

As regards the influence of alignment in collagen fibrils, from Fig. 6 and Table 4 it follows that the longitudinal elastic modulus increased markedly -but the transverse modulus decreased very slightly- with grouping of collagen fibrils in a specific direction (i.e., at low γ_2 values). Therefore, woven tissue becomes stiffer in the longitudinal direction as collagen fibrils align. Fibril alignment has been observed in woven tissue of human foetuses (Su et al, 1997), but not in bone callus. As can also be seen from Fig. 6, tissue stiffness increased with increasing ash fraction as a result of water being gradually replaced with a stiffer material (hydroxyapatite mineral).

Su et al (1997) examined femur diaphyses in human foetuses of variable gestational age (14-26 weeks). This tissue is microstructurally similar to woven tissue forming on bone callus after a fracture (McKibbin, 1978; Frost, 1989a,b; Wen et al, 1995), so it allows extrapolation of the results obtained with the proposed micromechanical model. The longitudinal Young's modulus for 26-week-old foetuses ranged from 9 GPa in the periosteum to 16 GPa in the endosteum. The difference arose from the way tissue forms during foetal bone development: from the inside to the outside. Thus, the endosteum is older and contains greater amounts of mineral as a result (Su et al, 1997). The proposed model estimated E_l ranging from 9 GPa at $\alpha = 0.511$ to 16 GPa at $\alpha = 0.580$, the former value being consistent with the experimentally found composition in sheep (García-Rodríguez, 2014) and the latter being a moderate estimate of mineral content. No higher mineral contents were analysed as they are unlikely to be reached by so young foetuses. As can be seen from figs. 6 and 7, stiffness in the longitudinal direction increased markedly with increasing ash fraction, much more markedly than in the transverse direction. In any case, the Young's modulus of foetal woven tissue is smaller than that of lamellar tissue; in fact, the latter ranges from 18 to 25 GPa depending on the mineral content, which can be much higher in old lamellar tissue.

This result raises an interesting question: why is the stiffness of woven bone so small compared to that of lamellar tissue? and, more precisely, from all the microstructural differences between both, which are the most influential factors? Probably, the composition and the orientation of collagen fibrils. Let us study the composition first. Mineral is the stiffest phase in bone and the mineral contents analyzed in this paper were much lower than the typical

values for lamellar tissue.[1] However, it can be thought that, even when woven tissue gets saturated with mineral, it will be less rigid than lamellar tissue, given that its collagen concentration is higher (recall Table 2).

The special microstructure of woven bone has also an important effect on its stiffness. This microstructure, modelled in the present paper, was compared with that of lamellar tissue considered in a previous work (Martínez-Reina et al, 2011). This was done by applying the present model with the volumetric composition of human lamellar tissue (see Table 2) and comparing the results with those obtained in that previous work (with the composition and microstructure of lamellar tissue). The latter provided an orthotropic material with Young's moduli: $E_1 = 17.2\,GPa$, $E_2 = 19.7\,GPa$, $E_3 = 22.0\,GPa$ (Martínez-Reina et al, 2011). Meanwhile, a quasi-isotropic ($\gamma_2 = \pi/2$) woven bone with the same composition would have a Young's modulus $E = 3.65\,GPa$, i.e. stiffer than woven bone with its actual composition ($E = 1.90\,GPa$), but much more flexible than lamellar bone. This difference highlights the importance of the hierarchical and well organized microstructure of lamellar bone in its mechanical features and is explained by two reasons. On the one hand, the high stiffness of the mineralized collagen fibril in the longitudinal direction as compared with the transverse direction. On the other hand, a uniform distribution of the fibril orientation gives more weight to the most flexible direction, in the sense of a Reuss average. Thus, a uniform distribution in the three directions ($\gamma_2 = \pi/2$) yields a quasi-isotropic material with a flexibility similar to that of the collagen fibril in the transverse direction.

In addition, a quasi-aligned woven bone ($\gamma_2 = \pi/18$) with the composition of lamellar tissue would be very stiff in the longitudinal direction ($E_l = 27.1\,GPa$) and very flexible in the transversal direction ($E_t = 2.59\,GPa$). In this case, the uniform distribution of fibrils' orientation in the transverse plane (implicit in the present model by assuming $\rho(\mathbf{g})$ to be independent of ϕ_1) yields a transversely isotropic material with a very low transverse stiffness. In contrast, the longitudinal modulus, $E_l = 27.1\,GPa$, would be higher than any modulus in the lamellar tissue since, in the latter, the lamellae were superimposed in layers by rotating the orthotropic lamellar tissue in three perpendicular directions (see Martínez-Reina et al (2011) for details). Again, this superimposition results in an averaged stiffness that reduces the differences between the stiffest and the most flexible directions.

The predominance of the most flexible direction in the homogenization process also explains the little variation of the transverse stiffness with $gamma_2$ (see fig. 6). In the quasi-aligned case the transverse stiffness of the tissue almost coincides with that of the fibrils, very low. As $gamma_2$ rises, some fibrils begin to be aligned with the transverse direction, contributing with their high longitudinal stiffness to the transverse stiffness of the composite. However, the stiffness of those fibrils is *overshadowed* by the high transverse flexibility of

[1] This was so due to the commented time limitation of the model, which makes it inapplicable well before the tissue is saturated with mineral.

the other fibrils, aligned with the longitudinal direction, so that the increase in transverse stiffness is negligible.

Other features that are different between woven and lamellar tissue are the porosity and the aspect ratio of mineral crystals. The typical dimensions of mineral crystals are different though quite similar: $a = 32\,nm$, $b = 19\,nm$, $c = 3\,nm$ in human foetal woven bone (Su et al, 2003) versus $a = 50\,nm$, $b = 25\,nm$, $c = 3\,nm$ (Rho et al, 1998) in lamellar bone, which translates into a minimal influence in the modelled stiffness. The porosity could indeed play a distinguishing role, but despite being different, its value is so small in both tissues that its influence on the stiffness is negligible as well. Dwelling on this idea, the vascular porosity was not included in the model in spite of being present in the woven tissue, as analyzed in a related work (Mora-Macías, 2016). It was excluded because the incipient vessels are so scarce at the time interval this model is valid that its effect would be negligible.

The Young's modulus of collagen adopted here (in the order of 1 GPa, see Table 1) is roughly ten times lower than that measured by Cusack and Miller (1979) in rat-tail tendons and used in some similar works (Hellmich et al, 2004; Tiburtius et al, 2014). Given that collagen is the most abundant constituent in woven tissue, (see Table 2), increasing its stiffness by a factor of 10 leads to an increase in the composite's stiffness by approximately the same factor. This would result in an abnormally high stiffness of woven bone, no matter the homogenization scheme followed, and not matching the experimental evidence. This suggests that the stiffness measured by Cusack and Miller (1979) was likely overestimated and that the collagen stiffness must be in the order of 1 GPa as other works have proposed (see Bonfield and Li (1967); Currey (1969); Geoffrey (1972); Mitchel and Burr (1988); Sasaki et al (1989); Crolet et al (1993); Yoon and Cowin (2008b) among many others.)

The main limitation of the proposed model arises from the assumed microstructure of woven tissue. In fact, collagen fibrils are known to be highly disordered, probably because the tissue forms very rapidly; however, the exact orientation of the fibrils is unknown. In this work, we assumed fibrils to be uniformly randomly arranged, which was a major simplification. Also, the geometry of hydroxyapatite crystals was greatly simplified by assuming an ellipsoidal shape, an acceptable simplification given that the presence of impurities make crystals highly amorphous and rather variable in morphology. Other major limitations of the proposed micromechanical model include assuming that (a) water partitioning between collagen and mineral to form the wet phases (see Eq. (7)) and (b) the combined volume of the lacuna and canaliculi in each unit cell (see Eq. (26)), are identical in woven and lamellar tissue. These simplifications were imposed by the lack of specific information for woven tissue and the need to replace it with known data for lamellar tissue (Martínez-Reina et al, 2011). Nevertheless, they have little effect on the results.

5 Conclusions

To the authors' knowledge, no multiscale micromechanical model for the elastic properties of woven bone tissue has been reported to date. The proposed model depends on the composition of woven tissue, which changes during mineralization, and on the potential alignment of collagen fibrils as observed in foetal woven tissue (Su et al, 1997).

The model was used to estimate the elastic constants of callus woven tissue (specifically, callus resulting from sheep bone transport, the composition of which was determined in a previous work). The stiffness tensor obtained was quasi-isotropic and the Young's modulus, 1.9 GPa, similar to the experimental values for fracture calluses in other species.

The model was also used to estimate the elastic constants of foetal woven tissue, where collagen fibrils are slightly aligned. The resulting stiffness tensor was quasi-transversely isotropic and the longitudinal Young's modulus ranged from 9 to 16 GPa depending on the mineral content. These values are smaller than those for lamellar tissue but similar to those found by Su et al (1997) in human foetuses.

References

Beno T, Yoon Y, Cowin S, SPFritton (2006) Estimation of bone permeability using accurate microstructural measurements. J Biomech 39(13):2378–2387

Benveniste Y (1990) Some remarks on three micromechanical models in composite media. J Appl Mech-T ASME 57(2):474–476

Bonfield W, Li E (1967) Anisotropy of nonelastic flow in bone. J Appl Phys 38:2450–2455

Brighton C, Hunt R (1986) Histochemical localization of calcium in the fracture callus with potassium pyroantimonate: possible role of chondrocyte mitochondrial calcium in callus calcification. J Bone Joint Surg Am 68-A(5):703–715

Brighton C, Hunt R (1997) Early histologic and ultrastructural changes in microvessels of periosteal callus. J Orthop Trauma 11(4):244–253

Buckwalter J, Glimcher M, Cooper R, Recker R (1995) Bone biology. Part I: structure, blood supply, cells, matrix, and mineralization. J Bone Joint Surg Am 77(8):1256–1275

Bunge H (1982) Texture analysis in materials science: mathematical methods. Butterworths

Chou P, Carleone J, Hsu C (1972) Elastic constants of layered media. J Compos Mater 6(1):80–93

Cowin S (1999) Bone poroelasticity. J Biomech 32:217–238

Cowin S, Yang G, Mehrabadi M (1999) Bounds on the effective anisotropic elastic constants. J Elasticity 57(1):1–24

Crolet J, Aoubiza B, Meunier A (1993) Compact bone: numerical simulation of mechanical characteristics. J Biomech 26(6):677–687

Currey J (1969) The relationship between the stiffness and the mineral content of bone. J Biomech 2:477–480

Cusack S, Miller A (1979) Determination of the elastic constants of collagen by brillouin light scattering. J Mol Biol 135:39–51

Deuerling J, Yue W, Espinoza Orías A, Roeder R (2009) Specimen-specific multi-scale model for the anisotropic elastic constants of human cortical bone. J Biomech 42(13):2061–2067

Dong X, Guo X (2006) Prediction of cortical bone elastic constants by a two-level micromechanical model using a generalized self-consistent method. J Biomech Eng-T ASME 128(3):309–316

Eshelby J (1957) The determination of the elastic field of an ellipsoidal inclusion, and related problems. Proc R Soc Lon Ser-A 241(1226):376–396

Farlay D, Panczer G, Rey C, Delmas P, Boivin G (2010) Mineral maturity and crystallinity index are distinct characteristics of bone mineral. J Bone Miner Metab 28:433–445

Ferrari M, Johnson G (1989) Effective elasticities of short-fiber composites with arbitrary orientation distribution. Mech Mater 8(1):67–73

Fritsch A, Hellmich C (2007) 'Universal' microstructural patterns in cortical and trabecular, extracellular and extravascular bone materials: Micromechanics-based prediction of anisotropic elasticity. J Theor Biol 244(4):597–620

Fritsch A, Dormieux L, Hellmich C (2006) Porous polycrystals built up by uniformly and axisymmetrically oriented needles: homogenization of elastic properties. CR Mecanique 334:151–157

Fritsch A, Hellmich C, Young P (2013) Micromechanics-derived scaling relations for poroelasticity and strength of brittle porous polycrystals. J Appl Mech 80:020,905

Frost H (1989a) The biology of fracture healing. An overview for clinicians. Part I. Clin Orthop Relat Res 248:283–293

Frost H (1989b) The biology of fracture healing. An overview for clinicians. Part II. Clin Orthop Relat Res 248:294–309

García-Aznar J, Rueberg T, Doblaré M (2005) A bone remodelling model coupling microdamage growth and repair by 3D BMU-activity. Biomech Model Mechan 4:147–167

García-Rodríguez J (2014) Modelo de remodelación de callo óseo de fractura de fémur humano. PhD thesis, Universidad de Sevilla, Seville (Spain)

Gardner T, Stoll T, Marks L, Mishra S, Knothe Tate M (2000) The influence of mechanical stimulus on the pattern of tissue differentiation in a long bone fracture - A FEM study. J Biomech 33(4):415–425

Geoffrey H (1972) The Biochemistry and Physiology of Bone, Vol. 1. Academic Press, New York.

Ghanbari J, Naghdabadi R (2009) Nonlinear hierarchical multiscale modeling of cortical bone considering its nanoscale microstructure. J Biomech 42(10):1560–1565

Gong J, Arnold J, Cohn S (1964) Composition of trabecular and cortical bone. Anat Rec 149:325–332

Grant C, Brockwell D, Radford S, Thomson N (2009) Tuning the elastic modulus of hydrated collagen fibrils. Biophys J 97:2985–2992

Hashin Z (1968) Assessment of the self-consistent scheme approximation. J Compos Mater 2:284–300

Hellmich C, Ulm FJ (2002) Micromechanical model for ultrastructural stiffness of mineralized tissues. J Eng Mech-ASCE 128(8):898–908

Hellmich C, Barthélémy JF, Dormieux L (2004) Mineral-collagen interactions in elasticity of bone ultrastructure - A continuum micromechanics approach. Eur J Mech A-Solid 23(5):783–810

Hernandez C, Beaupré G, Keller T, Carter D (2001a) The influence of bone volume fraction and ash fraction on bone strength and modulus. Bone 29(1):74–78

Hernandez C, Beaupré G, Marcus R, Carter D (2001b) A theoretical analysis of the contributions of remodeling space, mineralization, and bone balance to changes in bone mineral density during alendronate treatment. Bone 29(6):511–516

Hernandez C, Majeska R, Schaffler M (2004) Osteocyte density in woven bone. Bone 35(5):1095–1099

Hill R (1965) A self consistent mechanics of composite materials. J Mech Phys Sol 13:213–222

Hunt R (Accessed 10 March 2016) Material interaction varies bone strength: mammals. http://www.asknature.org/strategy/6bc0469baa23a29a6b5f9eb6febb75a8

Jackson S, Cartwright A, Lewis D (1978) The morphology of bone mineral crystals. Calcif Tissue Int 25:217–222

Katz J (1968) Hard tissue as a composite material - I. Bounds on the elastic behavior. J Biomech 4:455–473

Kotha S, Guzelsu N (2007) Tensile behavior of cortical bone: dependence of organic matrix material properties on bone mineral content. J Biomech 40(1):36–45

Lees S, Heeley J, Cleary P (1979) A study of some properties of a sample of bovine cortical bone using ultrasound. Calcif Tissue Int 29(2):107–117

Leong P, Morgan E (2008) Measurement of fracture callus material properties via nanoindentation. Acta Biomater 4:1569–1575

López-Pliego E, Giráldez-Sánchez M, Mora-Macías J, Reina-Romo, Domínguez J (2015) Histological evolution of the regenerate during bone transport. Experimental study in sheep. Injury (under review)

Martínez-Reina J, Domínguez J, García-Aznar J (2011) Effect of porosity and mineral content on the elastic constants of cortical bone: a multiscale approach. Biomech Model Mechan 10(3):309–322

McKibbin B (1978) The biology of fracture healing in long bones. J Bone Joint Surg Br 60 B(2):150–162

Mitchel B, Burr D (1988) Stiffness of compact bone. effect of porosity and density. J Biomech 21:13–16

Mora-Macías J (2016) Biomechanics of bone transport: in vivo, ex vivo and numerical characterization. PhD thesis, Universidad de Sevilla, Seville (Spain)

Mora-Macías J, Reina-Romo E, Domínguez J (2016) Model of the distraction callus tissue behavior during bone transport based in experiments in vivo. J Mech Behav Biomed Mater 61:419–430

Nemat-Nasser S, Hori M (1999) Micromechanics: overall properties of heterogeneous materials. Elsevier

Parfitt A (1987) Bone remodeling and bone loss: understanding the pathophysiology of osteoporosis. Clin Obstet Gynecol 30(4):789–811

Pettermann H, Böhm H, Rammerstorfer F (1997) Some direction-dependent properties of matrix-inclusion type composites with given reinforcement orientation distributions. Compos Part B-Eng 28(3):253–265

Porter D (2004) Pragmatic multiscale modelling of bone as a natural hybrid nanocomposite. Mat Sci Eng A-Struct 365(1-2):38–45

Remaggi F, Canè V, Palumbo C, Ferretti M (1998) Histomorphometric study on the osteocyte lacuno-canalicular network in animals of different species. I. Woven-fibered and parallel-fibered bones. Ital J Anat Embryol 103(4):145–155

Rho J, Kuhn-Spearing L, Zioupos P (1998) Mechanical properties and the hierarchical structure of bone. Med Eng Phys 20:92–102

Sasaki N, Matsushima N, Ikawa T, Yamamura H, Fukuda A (1989) Orientation of bone mineral and its role in the anisotropic mechanical properties of bone transverse anisotropy. J Biomech 22:157–164

Sevostianov I, Kachanov M (2000) Impact of the porous microstructure on the overall elastic properties of the osteonal cortical bone. J Biomech 33(7):881–888

Sfeir C, Ho C, Doll B, et al (2005) Fracture repair. In: Lieberman J, Friedlaender G (eds) Bone regeneration and repair, Totowa: Humana Press, Inc., pp 21–43

Smith J (1960) Collagen fibre patterns in mammalian bone. J Anat 94(3):329–344

Su X, Feng Q, Cui F, Zhu X (1997) Microstructure and micromechanical properties of the mid-diaphyses of human fetal femurs. Connect Tissue Res 36(3):271–286

Su X, Sun K, Cui F, Landis W (2003) Organization of apatite crystals in human woven bone. Bone 32(2):150–162

Tiburtius S, Schrof S, Molnár F, Varga P, Peyrin F, Grimal Q, Raum K, Gerisch A (2014) On the elastic properties of mineralized turkey leg tendon tissue: multiscale model and experiment. Biomech Model Mechanobiol 13(5):1003–1023

Vetter A, Epari D, Seidel R, Schell H, Fratzl P, Duda G, Weinkamer R (2010) Temporal tissue patterns in bone healing of sheep. J Orthop Res 28(11):1440–1447

Vetter A, Liu Y, Witt F, et al (2011) The mechanical heterogeneity of the hard callus influences local tissue strains during bone healing: a finite element study based on sheep experiments. J Biomech 44(3):517–523

Wang L, Fritton S, Cowin S, Weinbaum S (1999) Fluid pressure relaxation depends upon osteonal microstructure: modeling of an oscillatory bending

experiment. J Biomech 32:663–672
Wen H, Cui F, Feng Q, Li H, Zhu X (1995) Microstructural investigation of the early external callus after diaphyseal fractures of human long bone. J Struct Biol 114(2):115–122
Yang G, Kabel J, Van Rietbergen B, Odgaard A, Huiskes R, Cowin S (1998) Anisotropic Hooke's law for cancellous bone and wood. J Elasticity 53(2):125–146
Yoon Y, Cowin S (2008a) An estimate of anisotropic poroelastic constants of an osteon. Biomech Model Mechan 7(1):13–26
Yoon Y, Cowin S (2008b) The estimated elastic constants for a single bone osteonal lamella. Biomech Model Mechan 7(1):1–11
Yoon Y, Yang G, Cowin S (2002) Estimation of the effective transversely isotropic elastic constants of a material from known values of the material's orthotropic elastic constants. Biomech Model Mechan 1(1):83–93
Zhang D, Cowin S (1994) Oscillatory bending of a poroelastic beam. J Mech Phys Solids 42:1575–1599
Zhang D, Weinbaum S, Cowin S (1998) Estimates of the peak pressure in bone pore water. J Biomech Eng 120:697–703
Zhou H, Shen V, Dempster D, Lindsay R (2001) Continuous parathyroid hormone and estrogen administration increases vertebral cancellous bone volume and cortical width in the estrogen-deficient rat. J Bone Miner Res 16:1300–1307